

# Programming Diffusion and Localization of DNA Signals in 3D-Printed DNA-Functionalized Hydrogels

Julia Müller, Anna Christina Jäkel, Dominic Schwarz, Lukas Aufinger, and Friedrich C. Simmel\*

Additive manufacturing enables the generation of 3D structures with predefined shapes from a wide range of printable materials. However, most of the materials employed so far are static and do not provide any intrinsic programmability or pattern-forming capability. Here, a low-cost 3D bioprinting approach is developed, which is based on a commercially available extrusion printer that utilizes a DNA-functionalized bioink, which allows to combine concepts developed in dynamic DNA nanotechnology with additive patterning techniques. Hybridization between diffusing DNA signal strands and immobilized anchor strands can be used to tune diffusion properties of the signals, or to localize DNA strands within the gel in a sequence-programmable manner. Furthermore, strand displacement mechanisms can be used to direct simple pattern formation processes and to control the availability of DNA sequences at specific locations. To support printing of DNA-functionalized gel voxels at arbitrary positions, an open source python script that generates machine-readable code (GCODE) from simple vector graphics input is developed.

## 1. Introduction

DNA has been successfully employed as a programmable molecular substrate for the realization of self-assembled nanostructures of almost arbitrary shape.<sup>[1–3]</sup> Furthermore, using its inherent information storage and processing capabilities, combined with processes such as DNA hybridization and strand displacement reactions, a large variety of sensors, actuators, molecular machines, and computers have been developed.<sup>[4]</sup> Based on these capabilities, the realization of DNA-based molecular materials with advanced mechanical and computational functions appears possible.<sup>[5]</sup> For instance, such materials could be designed to functionally differentiate, reconfigure, or change

their shape in response to complex environmental inputs.

One of the challenges for the application of DNA in the context of macroscopic materials is the integration of nanoscale DNA components at a much larger scale. While there has been remarkable progress in the realization of submillimeter-sized DNA crystals<sup>[6,7]</sup> or superstructures composed of DNA origami subunits,<sup>[8–10]</sup> it is not clear whether all-DNA crystalline materials will be feasible or useful.


Other attempts to utilize DNA hybridization interactions also at larger length scales were based on DNA-mediated colloidal assembly<sup>[11–17]</sup> or on the creation of amorphous DNA-based hydrogels. In colloidal assembly, DNA simply serves as a sequence-programmable “glue” that organizes nano- or even microparticles into large assemblies with crystalline order, whose symmetry is governed by the size of the colloids and

interparticle interactions such as DNA hybridization between complementary DNA linkers, van der Waals, or depletion forces.

In contrast to such structurally well-defined configurations, also a range of amorphous, hydrogel-like materials have been developed,<sup>[18,19]</sup> which include gels exclusively made from DNA,<sup>[18,20–28]</sup> but also other polymer hydrogels, which were chemically modified with DNA.<sup>[29–31]</sup> In several cases, DNA was simply used as a sequence-dependent crosslinker, while in other cases, DNA also provided biochemical functionality to the gels. For instance, gels modified with gene length DNA have been previously utilized for compartmentalized cell-free gene expression reactions.<sup>[32,33]</sup> Stimulus-dependent hybridization reactions were utilized to create DNA-modified gels with shape memory,<sup>[34]</sup> while in-gel hybridization chain reactions were shown to induce swelling and shape changes.<sup>[35]</sup>

Strand displacement techniques have also been utilized to implement a variety of dynamical pattern formation processes in DNA-functionalized gels. For instance, a DNA circuit-based “molecular edge detector” could be demonstrated that was capable of finding the edge between regions of a gel that were illuminated by UV light and dark regions.<sup>[36]</sup> A different system termed “gellular automata” consisted of arrays of reaction chambers, which were separated from each other by hydrogel walls. The chambers contained components of DNA strand displacement circuits and were able to communicate via diffusion of DNA signals across the gel walls. This capability could be used to program various patterns into the “gellular” arrays.<sup>[37]</sup>

J. Müller, A. C. Jäkel, D. Schwarz, L. Aufinger, Prof. F. C. Simmel  
TU Munich  
Physics Department  
Physics of Synthetic Biological Systems  
Am Coulombwall 4a, Garching 85748, Germany  
E-mail: simmel@tum.de

 The ORCID identification number(s) for the author(s) of this article can be found under <https://doi.org/10.1002/smll.202001815>.

© 2020 The Authors. Published by WILEY-VCH Verlag GmbH & Co. KGaA, Weinheim. This is an open access article under the terms of the Creative Commons Attribution License, which permits use, distribution and reproduction in any medium, provided the original work is properly cited.

DOI: 10.1002/smll.202001815

The functionality of DNA-modified gels can be further enhanced through utilization of physical structuring techniques. Schulman and co-workers used photolithography to create DNA-functionalized gels with a variety of shapes, and further used it to spatially define different dynamical functions within the gels.<sup>[35]</sup> This was utilized to swell or bend different parts of a gel structure in a sequence-addressable manner, indicating the great potential of this approach for soft robotic applications.

A more recent approach toward the precise control of material shapes is offered by additive manufacturing techniques, which in contrast to planar lithographic approaches allow the realization of almost arbitrary structures in three spatial dimensions. This ability is only limited by the spatial resolution of the particular technique used, which can range from macroscopic dimensions down to  $\approx 100$  nm for methods such as 3D laser lithography.<sup>[38]</sup> Next to conventional engineering applications that require the fabrication of rigid structures composed of polymers, metals, or other solid materials, there has been considerable interest in bioprinting techniques<sup>[39]</sup> with applications mainly envisioned for tissue engineering or the creation of artificial organs.<sup>[40]</sup> Bioprinting is conducted with “bioinks,”<sup>[41,42]</sup> which typically are biocompatible gels that may contain additional biomolecules such as extracellular matrix or other scaffold proteins, DNA-modified peptides,<sup>[31]</sup> or even cells.<sup>[40,43,44]</sup>

Until now, there have been only very few attempts to utilize 3D bioprinting techniques in a cell-free synthetic biology context, however. One notable example is the creation of tissue-like 3D materials from water-in-oil emulsion droplets utilizing the droplet interface bilayer (DIB) technique.<sup>[45,46]</sup> In a different approach, an additive technique was used to assemble DNA covered polystyrene beads using DNA as a sequence-programmable glue,<sup>[36]</sup> resulting in the first examples of millimeter-sized, 3D-printed colloidal gels held together via DNA base-pairing interactions.

For the present work, we combined concepts from dynamic DNA nanotechnology with 3D bioprinting, which allowed us to create 3D DNA-functionalized hydrogel structures on the millimeter to centimeter scale. To this end, we developed a dedicated bioink, which can be covalently modified with DNA molecules, and which can be printed with an extrusion-based 3D printer. Our bioink was optimized for biocompatibility, printability, and structural rigidity. For the printing process, we refurbished a commercially available, inexpensive polymer extrusion printer, for which we also developed easy-to-use open source software for the generation of GCODE from svg-representations of the target structures.

Using our system, we demonstrate various patterning and pattern formation modalities that utilize concepts from dynamic DNA nanotechnology: sequence-based diffusion control, generation of gradients and spatial patterns, and sequence-addressable sorting and localization of DNA signal molecules.

## 2. Results and Discussion

### 2.1. Development of Printable DNA-Functionalized Gels

#### 2.1.1. Bioink

In order to implement spatially organized dynamic DNA processes within 3D-printed gels, several technical challenges

had to be tackled. Specifically, we aimed at the development of a DNA-functionalized gel with high printability, good print fidelity, and also long-term stability. Furthermore, we strived for working with widely available biopolymer gels that naturally come with a good biocompatibility. In initial experiments with gels composed of only a single polymer component, we usually were able to implement only one of these properties, but not all of them at once. We therefore investigated the use of polymer mixtures, which allowed us to realize printability and stability together with the possibility for DNA functionalization. Our optimized bioink mixture consists of 10% gelatin, 3% alginate, and 1% low melting temperature agarose, which can be printed by extrusion at temperatures of  $42 \pm 2$  °C. Gelation of this material upon cooling leads to fast solidification (within 5–10 s) and high structural fidelity. Optionally, the alginate component of the print can be crosslinked by adding a  $100 \times 10^{-3}$  M CaCl<sub>2</sub> solution to ensure long-term stability.

#### 2.1.2. Bioprinter

In addition to the development of DNA-functionalized bioinks, we realized an easy-to-use bioprinter platform based on an inexpensive, commercially available extrusion printer (cf. **Figure 1A**; Section S4 and Figure S3, Supporting Information). In order to adjust the printer for our application, the main focus was put on the development of a printhead that can be loaded with small samples (with a targeted volume range from 0.1 to 1 mL) of modified bioink. Direct extrusion of the bioink can be achieved by either using compressed air or mechanical pressure to generate the extruding force. For our setup, we decided on a mechanical extrusion mechanism that required relatively low maintenance compared to air pressure extrusion. In order to overcome mechanical issues when coupling to the soft gel and also to avoid large sample volumes, a hydraulic coupling to an external syringe pump was established. With this mechanism, the syringe pump driving the hydraulic oil could be placed on the workbench next to the printer, which avoids additional weight on the printhead, while the sample volume can be kept low (typical volumes used were around 500  $\mu$ L). In contrast to extrusion systems driven by air pressure, the flow of the bioink can be terminated by a reversal of the hydraulic pressure and the bioink can be retracted, which also allows printing of discrete gel droplets. Our best printing results were achieved for prints with nozzles of inner diameters 200  $\mu$ m (G27) or 150  $\mu$ m (G30).

#### 2.1.3. Software

In order to enable printing of arbitrary structures independent of printer platform and commercial software, we developed an open source python script that generates machine-readable code (GCODE) for 3D printers on the basis of an input graphics file together with a text-based parameter file (Section S3 and Figures S1 and S2, Supporting Information). The input file provides the print layers as 2D vector graphics in svg-format, and therefore neither computer-aided design (CAD) software nor CAD design skills are required. The parameter file hands over all necessary printing parameters and also contains a record of

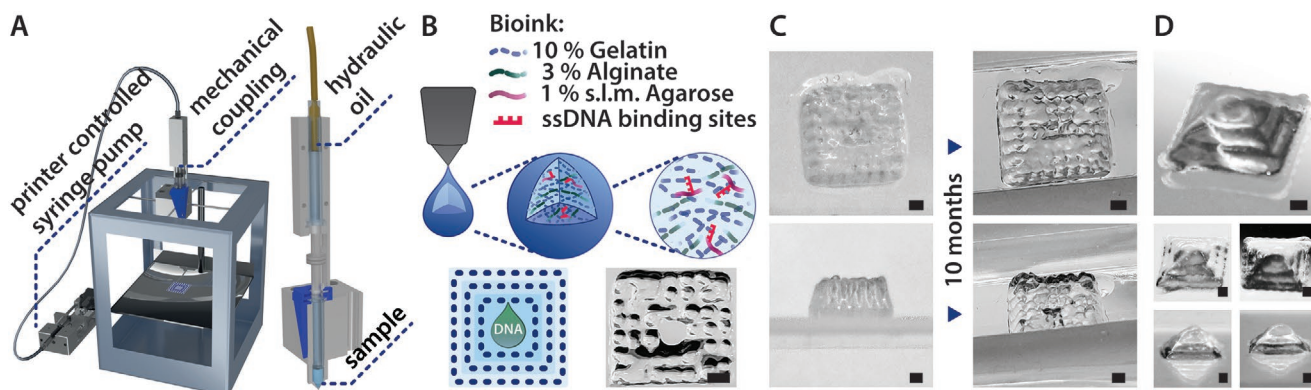


**Figure 1.** A) Bioprinter setup with an external syringe pump and hydraulic coupling to a syringe containing a small sample volume. The printhead can be equipped with up to four different syringes and functions as a thermoblock. The bioink is held at a constant temperature during extrusion. B) Our DNA bioink consists of three different polymer components: gelatin as the main component providing structural stability, alginate as a viscosity enhancer, and super low melt agarose as the DNA-functionalizable component. C) Long-term experiment demonstrating the stability of the bioink and the print: extruded structures remain stable in form and size over 10 months in a sealed container. Scale bar: 1 mm. D) Pyramid structures (I–III) printed with the bioink. Scale bar: 1 mm.

the experimental setup. Printing parameters include extrusion speed, nozzle diameter, print velocity, and optional correction functions, which can be included in the generated print file.

In usual 3D printing applications, a printable model of a 3D body is created using a CAD tool, which is then converted into a continuous spatial print trajectory using a slicing software. The printer path is selected based on the boundary conditions set by the slicer and cannot be modified in a commercial slicer software. In contrast to this approach—which always involves printing of continuous lines—we chose a voxel-based printing strategy, which makes it possible to place single gel droplets at specific locations. Our approach enables the precise arrangement of short lines in the 2D vector file of each layer that will be printed as single voxels. Specific locations can thus be reached and the printer pathway is defined by the order of the single points in the vector graphics file. Details on the bioprinting platform and software can be found in the Supporting Information. The source code (Python 3.0) is available on Github including example files (<https://github.com/julia-mueller/bioprinter/>).

#### 2.1.4. Gel Structures

The printed gel structures solidify on the glass substrate directly after extrusion by cooling to room temperature (the gel mixture was optimized to avoid additional cooling of the substrate). Structures with  $\approx 20$  print layers reach a height of  $\approx 10$  mm and remain stable in form for at least 10 months when sealed inside of a small glass or plastic container (see Figure 1). Shrinking of the gel structures due to drying was observed to occur only during the first 24 h after printing.

#### 2.1.5. Functionalization of the Bioink with Sequence-Addressable DNA Anchors

Most importantly for our application, the bioink can be functionalized with oligonucleotides, which can serve as sequence-addressable molecular “anchors” for DNA strands containing

complementary sequences. Functionalization is achieved via modification of the agarose component of the bioink as described previously<sup>[33]</sup>. Briefly, agarose is functionalized with alkyne groups using propargyl-isothiocyanate (PITC), and then coupled to azide-modified oligonucleotides using copper-catalyzed azide–alkyne cycloaddition (“click chemistry”). For this procedure, the number of resulting terminal alkynes per agarose subunit was previously estimated to be 0.1%, corresponding to a concentration of  $25 \times 10^{-6}$  M alkynes in 1 wt% agarose.<sup>[33]</sup> As our bioink also contains 1 wt% agarose, it is expected to have a similar functionalization density. We further assessed the pore size of the printed gels by evaluating the uptake of fluorescently labeled dextran molecules with different sizes. Our experiments indicate a molecular weight cut-off (MWCO) between 10 and 50 kDa, corresponding to a pore diameter in the range of 5–10 nm (cf. Section S5 and Figure S4 in the Supporting Information).

#### 2.2. Free Diffusion of DNA Signals in Printed Gel Structures

We first characterized free diffusion of single-stranded DNA molecules inside of our 3D-printed gels. To this end, we created a cuboid 3D print with a rectangular window in its center, which was used to supply DNA sample solutions from outside (Figure 2A). In order to be able to monitor diffusion within the gel, we fluorescently labeled 10 nucleotide (nt) and 20 nt long DNA strands  $\bar{Y}_{10}$  and  $\bar{Y}_{20}$  (Alexa 488 and Alexa 647, respectively), mixed them in bioink, and placed them into the central opening. Diffusion of the strands into the surrounding gel structures was then recorded over a time course of 24 h. We estimated the diffusion coefficients of the DNA strands from the variance of the corresponding fluorescence intensity profiles at different time points, which resulted in  $D \approx 12 \mu\text{m}^2 \text{s}^{-1}$  for  $\bar{Y}_{20}$  and a correspondingly larger coefficient ( $D \approx 43 \mu\text{m}^2 \text{s}^{-1}$ ) for  $\bar{Y}_{10}$ . Simulations of diffusion profiles in cylindrical geometry using these diffusion coefficients showed very good agreement with the experimentally obtained fluorescence profiles (cf. Figure 2C; Section S6, Supporting Information). Fluorescence correlation

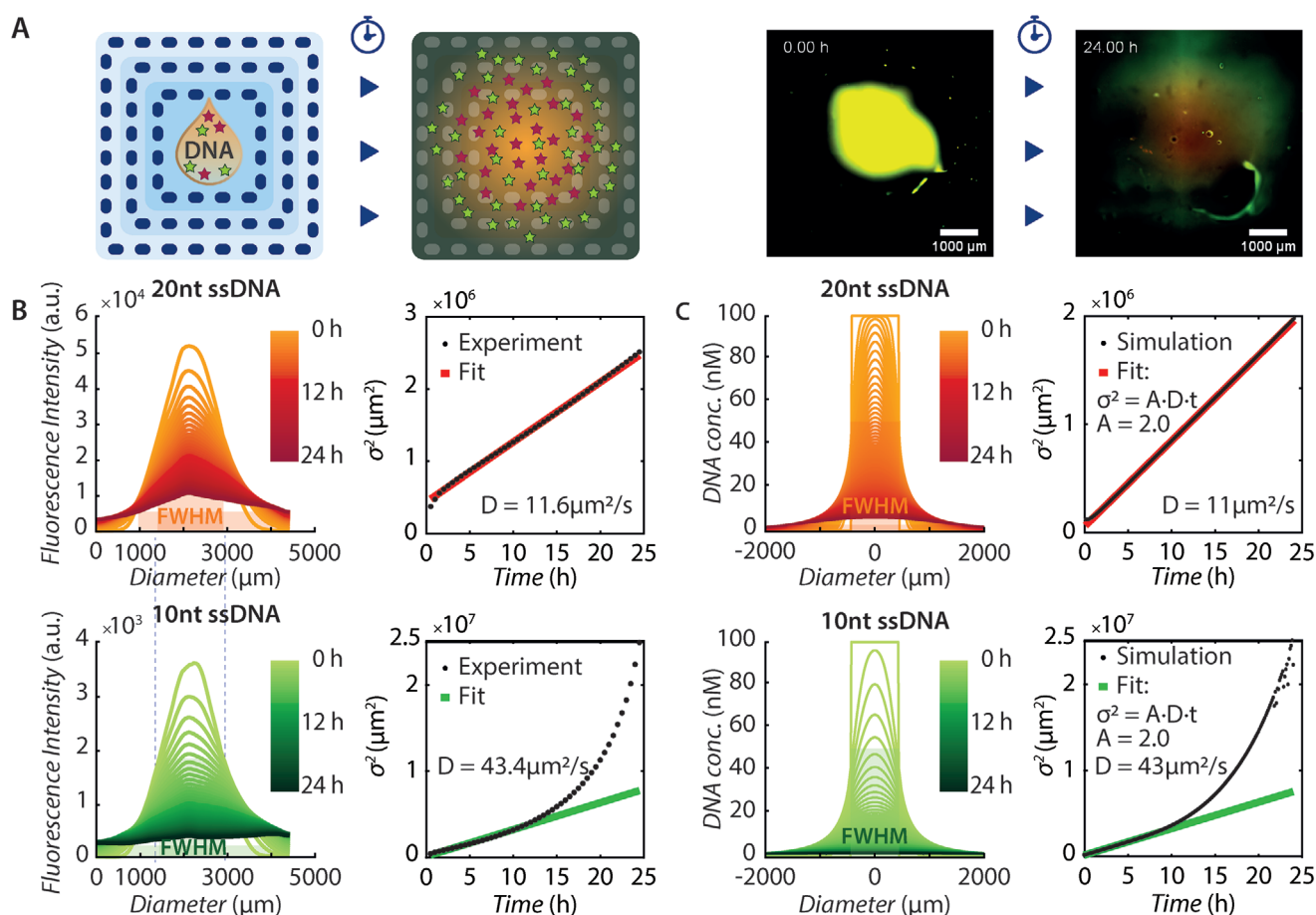


**Figure 2.** Diffusion of DNA molecules in a 3D-printed gel structure. A) Experimental setup: A drop of bioink containing DNA strands of 10 and 20 nt length (fluorescently labeled in Alexa 488 (green) and Alexa 647 (red), respectively) is added to the center of a 3D-printed cuboid test structure and the fluorescence intensities in the green and red channels are monitored over 24 h. B) Fluorescence profiles obtained from rectangular sections through the center of the print are analyzed as a function of time. The variances ( $\sigma^2$ ) of Gaussian fits to the experimental data are taken as approximate measures for the mean-squared displacement (MSD) of the diffusing molecules. Linear fits to  $\sigma^2 = 2 Dt$  yield the diffusion coefficients for the 20 and 10 nt long DNA strands (11.6 and  $43.4 \mu\text{m}^2 \text{s}^{-1}$ ). C) Simulated fluorescence profiles obtained from numerical solutions of the diffusion equation in cylindrical geometry using the experimentally obtained diffusion coefficients (for details see the Supporting Information). The striking deviation of the variance of the 10 nt long strands from the linear fit after  $\approx 10$  h is reproduced in the simulation and results from DNA strands reaching the boundaries of the printed structure.

spectroscopy studies on freely diffusing, unstructured oligonucleotides previously resulted in diffusion coefficients in the range of  $130\text{--}180 \mu\text{m}^2 \text{s}^{-1}$  for 20–10 nt long strands.<sup>[47]</sup> Diffusion is thus retarded up to ten times in our printed gels, but not completely suppressed, which is expected as the size of the diffusing DNA molecules is of the same order as the estimated pore size (see above).

### 2.3. Toehold-Mediated Strand Displacement (TMSD) and Localization of DNA in the Gel

We were next interested in utilizing the sequence-programmable interactions of diffusing DNA molecules with gel-immobilized DNA sequences to implement a variety of functional primitives for spatially distributed DNA circuits—namely, localized DNA strand displacement reactions, sequence-based control of diffusion, and sequence-directed molecular sorting.

In order to demonstrate an implementation of strand displacement reactions, we created a 3D-printed test object with unmodified bioink, into which we embedded a target pattern with DNA-functionalized ink in a second printing step (Figure 3A). The gel-localized DNA “anchor” strands ( $X_{20}$ ) were sequence-programmed to engage in a TMSD reaction with diffusible, double-stranded DNA constructs (“signal complexes”). A signal complex consisted of a fluorescently labeled DNA strand  $\bar{X}_{20}$  and a shorter, complementary strand labeled with a quencher,  $X_{14}\text{-Q}$ , exposing a 6 nt long single-stranded toehold on the fluorescent strand. Next, we applied a solution containing signal complexes on top of the print and allowed it to diffuse into the printed gel structure. In the mobile state, the fluorescence of the constructs is completely quenched, resulting in a very low fluorescent background signal in the gel. Upon interaction of a signal complex with an immobile DNA address, the quencher strand is displaced via TMSD, resulting in sequence-specific immobilization of the fluorescent signals

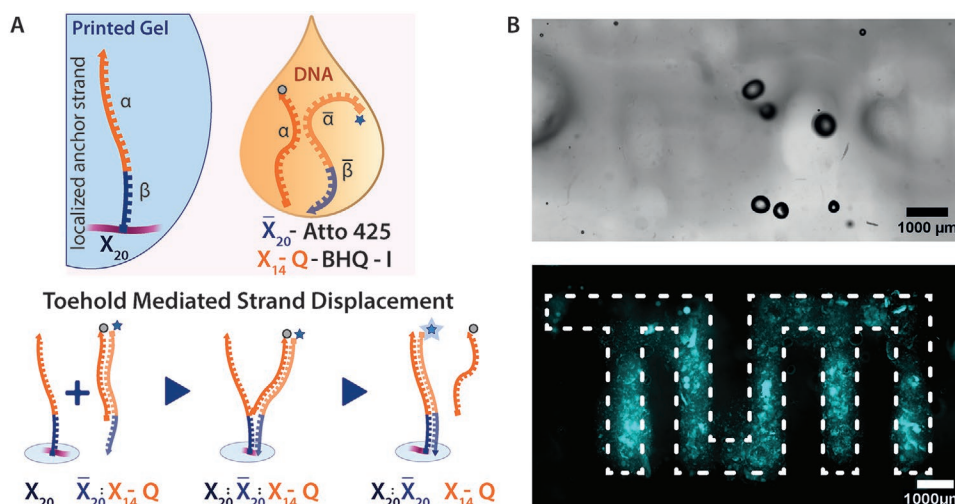


**Figure 3.** Spatially organized toehold-mediated strand displacement (TMSD) reactions inside a printed gel structure. A) Experimental scheme: The 20 nt long DNA anchor strands  $X_{20}$  are covalently immobilized in the printed gel. As diffusing signal molecules, DNA complexes composed of fluorescently labeled signal strands  $\bar{X}_{20}$  hybridized to quencher-labeled strands  $X_{14}$ -Q are added to the gel. The  $\bar{X}_{20}$ : $X_{14}$ -Q complexes have a 6 nt long ssDNA toehold, which facilitates TMSD of the quencher by the anchor strands. As a result, signal strands  $\bar{X}_{20}$  light up as soon as they are immobilized in the gel. B) Top: Microscopy image of a 3D-printed test structure with embedded anchor strand pattern (bottom view). Distinct areas are successively printed with unmodified and anchor modified bioink, respectively. Bottom: DNA signal complexes are added to the gel structure and allowed to freely diffuse through the gel. As a result, a fluorescent pattern (our University logo) emerges in the anchor modified regions (shown is an average image of four individual prints).

within the gel print (Figure 3B). In the experiment, the DNA signal complexes were initially applied centrally on top of the letters, after sealing of the whole structure with a thin layer of unmodified bioink. This resulted in a slightly inhomogeneous diffusion of the signals into the gel, causing the outer voxels of the letter T and M to exhibit a lower fluorescence than central areas of the logo.

#### 2.4. Sorting DNA Signals to Distinct Addresses

Our DNA bioprinter allows dropwise printing of bioinks functionalized with different DNA anchor strands at specific locations, enabling the sequence-programmable definition of more elaborate immobilization patterns. As an example, we printed a  $2 \times 2$  square (i.e.,  $2 \times 2$  cuboid) structure, in which each of the four corners of the structure contained one of two orthogonal ssDNA anchor strands ( $X_{20}$  and  $Y_{20}$ ). In a similar manner as in the localization experiment shown in Figure 3 (TUM logo), a bulk solution containing two orthogonal fluorophore-quencher duplex structures ( $\bar{X}_{20}$ : $X_{15}$ -Q and  $\bar{Y}_{20}$ : $Y_{14}$ -Q) was applied on top of the printed gel structure. Over the course of 10 h, the DNA solution unmixes and the DNA signals were sorted to their respective addresses (Figure 4).

#### 2.5. Sequence-Dependent Differential Diffusion

For many applications—in particular for the generation of spatiotemporal patterns via reaction-diffusion mechanisms—it will be necessary to tune the diffusion coefficient of the diffusing species. This may be achieved by

changing the gel density or viscosity of the medium, but these parameters are constrained by the requirement that the gel must be printable. Furthermore, these parameters globally affect all diffusing molecules in the gel. In the context of DNA-programmed circuits, an interesting alternative is given by the retardation of diffusing DNA strands by transient hybridization to immobile DNA anchor strands, which allows sequence-based control of the diffusion of individual DNA sequences through the gel.<sup>[36]</sup> In order to demonstrate the tunability of the effective diffusion coefficients, we designed a set of fluorescently labeled, 10 nt long DNA strands that had subsequences of 4, 6, 8, and 10 nt, which were complementary to corresponding subsequences of the gel-immobilized  $X_{20}$  anchor strands ( $\bar{X}_{10}$ -Alexa 647,  $\bar{X}_8$ +(dA)<sub>2</sub>-Alexa 488,  $\bar{X}_6$ +(dA)<sub>4</sub>-Atto 425,  $\bar{X}_4$ +(dA)<sub>6</sub>-TAMRA). An equimolar mixture of these strands was added to the center of an  $X_{20}$ -modified bioink gel structure and the fluorescent intensities were measured over 20 h (Figure 5; Figure S6, Supporting Information). As expected, transient hybridization of the diffusing strands to the anchors indeed leads to a reduction of the measured diffusion coefficients (Figure 5C). Longer regions of complementarity result in smaller off-rates of the bound strands, and thus reduced diffusion coefficients. While the  $\bar{X}_{10}$  strands thus have a very low effective diffusion coefficient of  $D \approx 1.4 \mu\text{m}^2 \text{s}^{-1}$ , the diffusion coefficients of the other strands range from  $\approx 30 \mu\text{m}^2 \text{s}^{-1}$  ( $\bar{X}_8$ ) over  $\approx 40 \mu\text{m}^2 \text{s}^{-1}$  ( $\bar{X}_6$ ) to  $\approx 120 \mu\text{m}^2 \text{s}^{-1}$  ( $\bar{X}_4$ ). Diffusion coefficients can thus be tuned via sequence over almost two orders of magnitude. Note that the diffusion coefficient for  $\bar{X}_4$  is larger than that of the freely diffusing 10 nt strand in Figure 2, which indicates a slight variability of the gel density from print to print, and potentially an influence of DNA secondary structure.

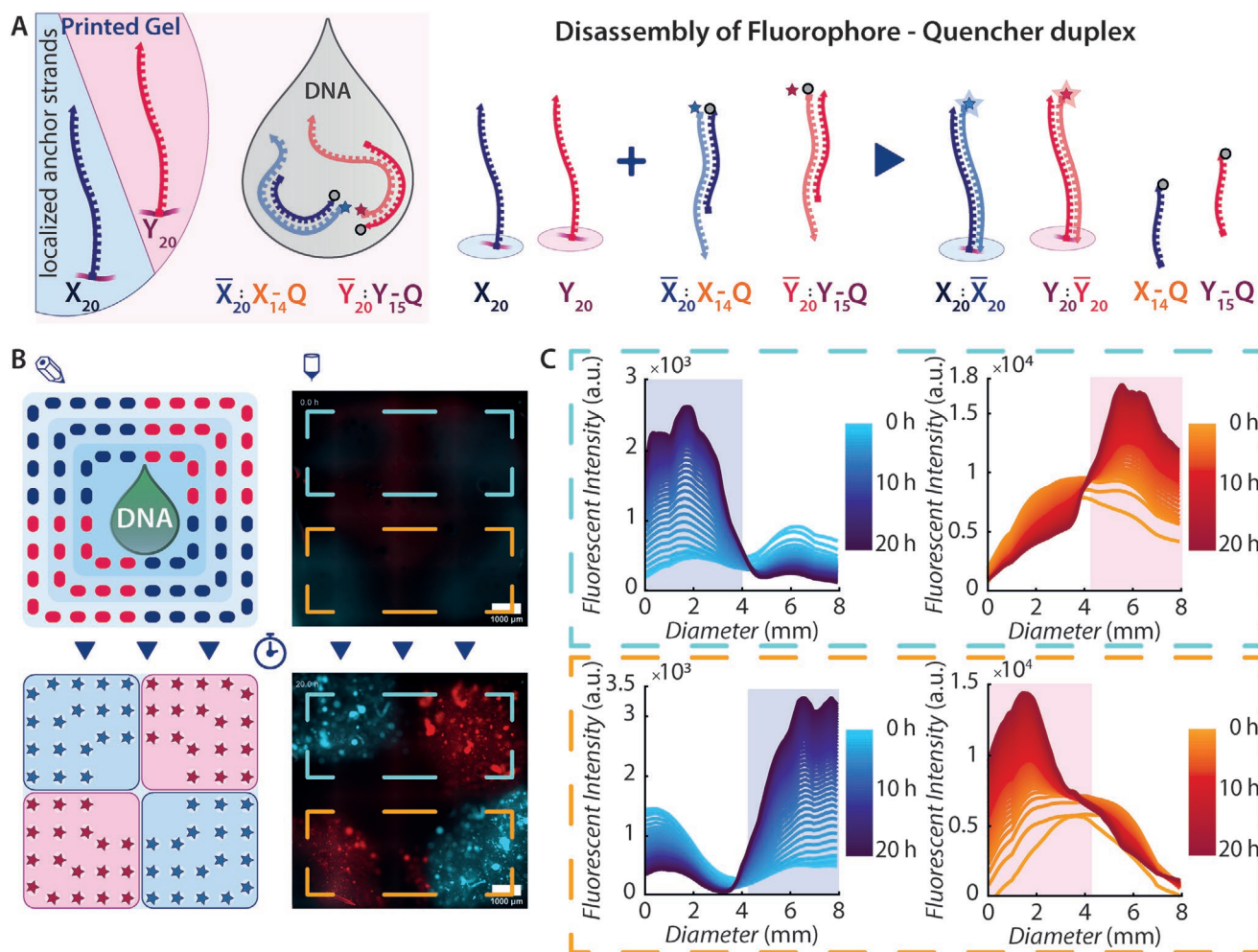


**Figure 4.** Sorting of DNA molecules to differently addressed regions within a gel print. A) The experimental scheme is analogous to Figure 3, but with two types of anchor strands ( $X_{20}$  and  $Y_{20}$ ) with orthogonal sequences, and two differently labeled signal complexes  $\bar{X}_{20}:X_{14}-Q$  and  $\bar{Y}_{20}:Y_{15}-Q$ , resulting in a localization of the labeled strands to different regions. B) As indicated in the scheme and shown in the fluorescence images, differently modified bioinks were printed in a  $2 \times 2$  checkerboard pattern. Quenched DNA signal complexes were then added to the print and allowed to diffuse into the gel over 20 h. C) Fluorescence profiles corresponding to the gel regions highlighted with the blue and orange boxes, showing sequence-programmed molecular sorting of the DNA signals over the time course of the experiment.

In contrast to the free diffusion experiments shown in Figure 2, due to their binding interactions, the strands in Figure 5 have a considerably lower free energy in the gel than outside, which effectively confines them to the gel region. As a result, the concentration at the gel boundaries is clamped to a low value, as can be seen from the plots of the fluorescence intensity in Figure 5B. This also causes the variance for the faster diffusing species to saturate at a value corresponding to the gel dimensions rather than to diverge as in Figure 2.

## 2.6. TMSD-Mediated Pattern Formation

Apart from transient binding of diffusing DNA strands to anchor strands, signal strands may also replace each other via toehold-mediated strand displacement reactions. Already in the experiments described in the previous section, strands

with longer complementarity regions were expected to displace bound strands with shorter complementary sequences. Similar reactions may also be used as the basis of simple pattern formation processes (Figure 6).

In order to demonstrate this capability, we added an equimolar mixture of 10 and 20 nt long signal strands ( $\bar{X}_{10}$  labeled with Alexa 647 and  $\bar{X}_{20}$  with Atto 425 fluorophores) in bioink to the central cavity of the printed scaffold structure and monitored their distribution over a time course of 20 h. As shown in Figure 6B, after  $\approx 6$  h a visible ring of Alexa 647-labeled DNA appeared around the central cavity. The temporal change of the fluorescence profiles indicates that the shorter  $\bar{X}_{10}$  strands moved into the gel more quickly, but also that short signals bound to anchors were later displaced by the slower  $\bar{X}_{20}$  strands with the higher binding affinity. Hence, the 20 nt strands barely move into the gel and are captured close to the center of the structure, whereas the shorter strands

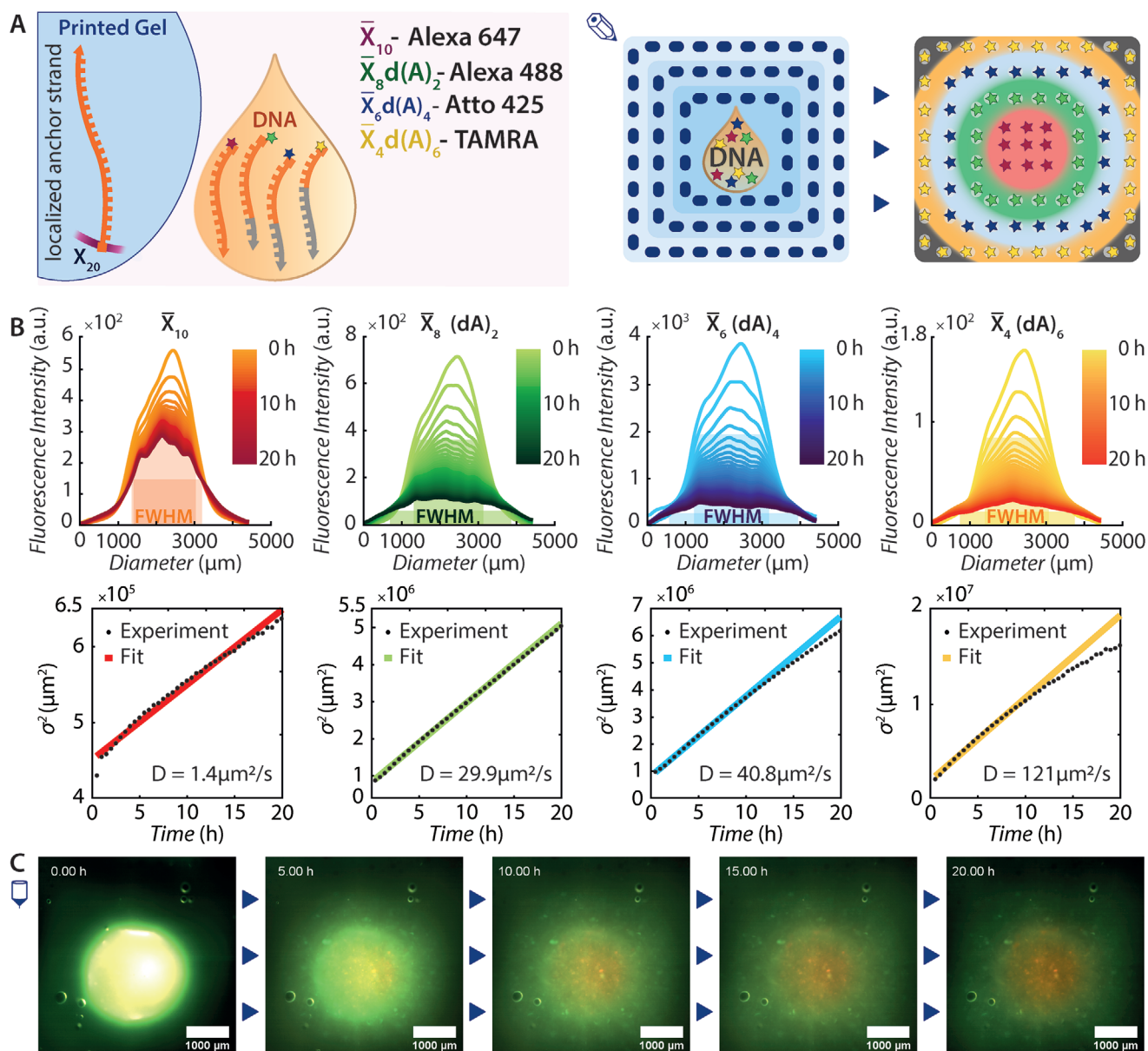


**Figure 5.** Sequence-tunable diffusion coefficients. A) In order to study how transient hybridization of DNA sequences to immobilized  $X_{20}$  anchor strands affects diffusion, a mixture of fluorescently labeled DNA strands with partial complementarity to the anchors was added in the center of a printed test structure. As indicated, we expected the strands with shorter complementarity regions to diffuse faster than those with longer regions, which is indeed observed in the experiments. B) Fluorescence profiles for the different DNA strands for different times and variation of the variance as a function of time. As expected, higher binding affinity leads to a lower diffusion coefficient and a more localized distribution of the respective DNA strands. In (C), microscopy images of the gel print for the indicated time points are shown in a superposition of all fluorescence channels (cf. Figure S6 in the Supporting Information for the separate fluorescence channels).

form a relatively well-defined ring localized around the core region. The results of the experiment may also be interpreted as “demixing” of a DNA sample, which results in a simple sequence-programmed reaction-diffusion pattern.

We next repeated the experiment with two 20 nt long DNA strands  $\bar{X}_{20}$  and  $\bar{X}_{10}+(dA)_{10}$ , which were expected to exhibit similar “free” diffusion coefficients. Again after  $\approx 6$  h a ring of fluorescently labeled DNA emerged around the center region (Figure 6C). As expected, the  $\bar{X}_{10}+(dA)_{10}$  strands moved into the

gel more slowly than the  $\bar{X}_{10}$  strands (cf. Figure 6B), while the  $\bar{X}_{20}$  strands displayed extremely retarded diffusion and barely entered the printed gel. As a result, the ring structure appeared with higher contrast than in the first experiment. The experimentally observed patterns can be very well reproduced using a simple reaction-diffusion model incorporating hybridization of the diffusing strands to the anchor strands and TMSD of shorter by longer strands (Figures S7 and S8, Supporting Information).

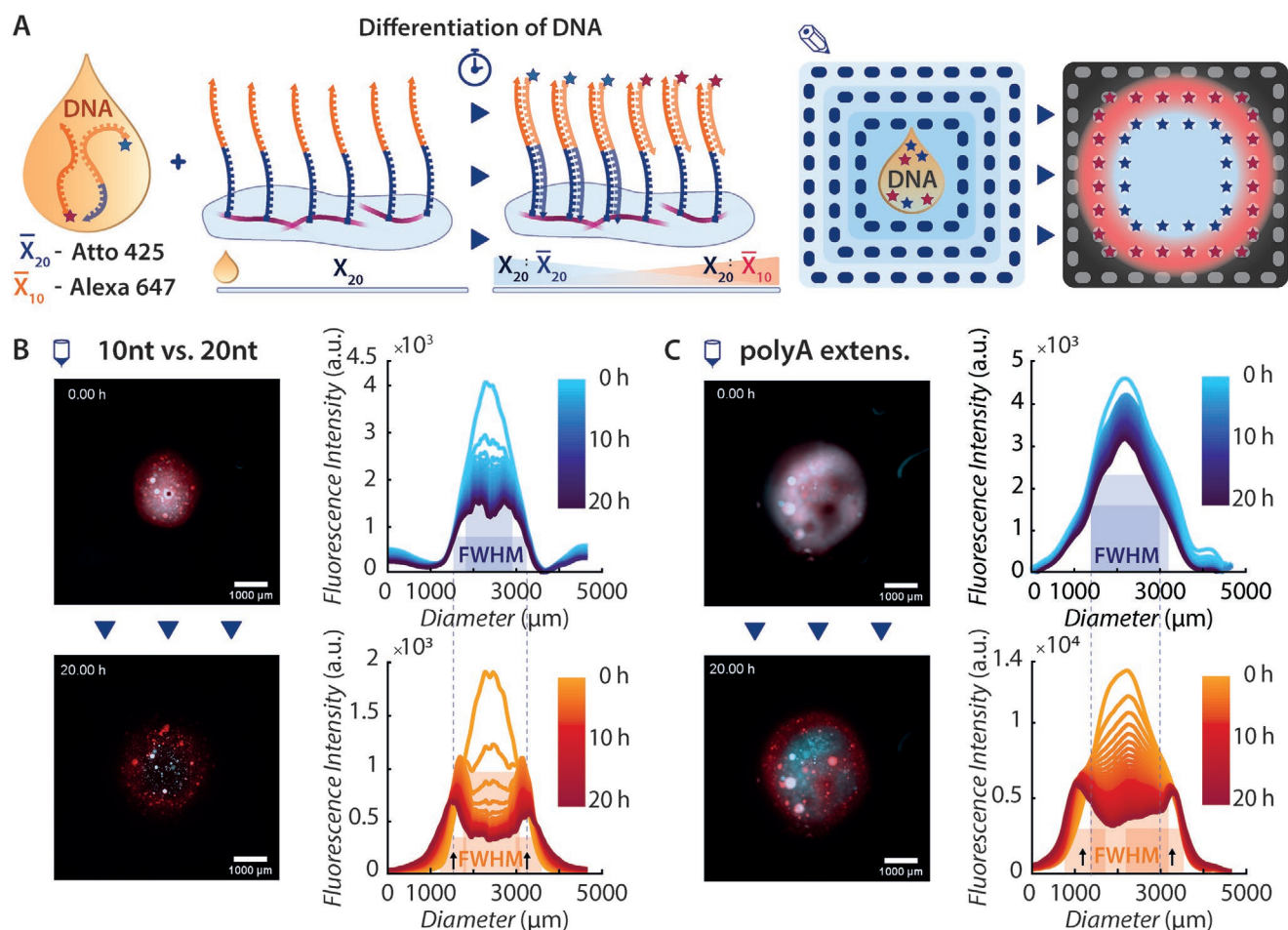


**Figure 6.** TMSD-based pattern formation in 3D-printed gels. A) As in the previous experiments described in Figures 3 and 4,  $X_{20}$  anchor strands are immobilized in the printed gel. DNA strands with different lengths of complementarity to  $X_{20}$  are then applied to the center of the gel print. Shorter/less complementary  $\bar{X}_{10}$  strands are expected to diffuse into the gel faster than  $\bar{X}_{20}$  strands. Furthermore,  $\bar{X}_{20}$  are expected to displace anchor-bound  $\bar{X}_{10}$  via toehold-mediated strand displacement, resulting in different gradients for  $\bar{X}_{20}$  and  $\bar{X}_{10}$  strands throughout the gel. B) Microscopy images (bottom view) of reaction-diffusion patterns generated by  $\bar{X}_{10}$  and  $\bar{X}_{20}$  strands in a 3D-printed hydrogel structure with homogeneously attached  $X_{20}$  anchors and corresponding fluorescence profiles for different time points. Due to the larger diffusion coefficient and reduced affinity to the anchor, a circular ring structure is created by the Alexa647-labeled  $\bar{X}_{10}$  strands (red) after a few hours. C) The same experiment as in (B) performed with two DNA signals of the same length ( $\bar{X}_{20}$  and  $\bar{X}_{10}$ - $(dA)_{10}$ ), but with different binding affinities to the anchors. The diffusion of the  $\bar{X}_{10}$ - $(dA)_{10}$  strands into the gel is reduced compared to the  $\bar{X}_{10}$  strands of (B), and thus the ring is more localized to the center. In consequence, diffusion of  $\bar{X}_{20}$  into the gel is reduced, resulting in a more sharply defined localization pattern.

### 3. Conclusion and Outlook

We have developed a low-cost bioprinting approach based on an affordable commercial extrusion printer, which was specifically optimized for the utilization of a DNA-functionalized bioink. Our bioink consists of a mixture of gelatin, alginate, and agarose, which was tuned to be printable at 42 °C and to solidify at room temperature within seconds. The agarose component can be functionalized with DNA using a click-chemistry-based protocol. The precise positioning capability of the printer facilitates the creation of DNA-labeled gel voxels within a larger hydrogel environment.

As a result, printed DNA scaffold structures can be used to immobilize DNA or potentially DNA-functionalized components in 3D in a sequence-addressable manner. Furthermore, we have shown that the size of the DNA signal molecules as

well as transient hybridization between the signals and gel-immobilized anchor strands can be used to control the diffusion coefficients of DNA strands over at least two orders of magnitude.

The combination of 3D bioprinting techniques with dynamic DNA nanotechnology opens up the possibility to utilize concepts borrowed from molecular programming in the context of 3D biomaterials, and on a length scale of several 100  $\mu\text{m}$ . Possible future applications of such 3D-printed structures include the realization of self-differentiating, soft biomaterials, or the development of scaffold structures that can be used to immobilize DNA-tagged components in biocompatible 3D environments. It is conceivable that reaction-diffusion and enzyme-assisted processes can be used to further refine and remodel 3D-printed structures and to create nontrivial chemical patterns within soft 3D prints.



## 4. Experimental Section

**Bioprinter:** An Ultimaker Original+ printer was utilized as the 3D positioning platform and was equipped with a custom-made printhead, onto which two sample syringes could be mounted (cf. Supporting Information for a detailed description). The temperature of the bioink samples contained in the syringes was controlled by an external control unit. Custom fabricated syringe pumps were placed on the workbench next to the printer and linked to the sample syringes in the heated printhead via a hydraulic coupling mechanism, which enabled retraction and synchronized extrusion directly controlled by the printer hardware. The approach allowed precise control over bioink flow and prevented mismatched timing of extrusion and positioning and uncontrolled continuous sample flow. The setup thus facilitated nanoliter-precise drop-on-demand extrusion of single droplets rather than continuous flow printing. Printing fidelity is improved when printing in a high humidity environment, which was realized by encapsulating the 3D printer into a poly(methyl methacrylate) housing that prevented extruded bioink from drying. The printer was controllable via program scripts written in the commonly used GCODE data format. Next to the print files generated with the in-house developed software also GCODEs generated by conventional 3D slicing software could be loaded.

**Bioink:** To ensure biocompatibility of the bioink (also in view of potential applications), the focus was on natural polymers without any added synthetic components. In the bioink mixture, 10% (w/v) gelatin (G1890, Sigma, Germany) was responsible for structural stability and fast gelation after extrusion. Alginate (9189.1, Carl Roth, Germany) was added at 3% (w/v) as a viscosity enhancer and to induce shear thinning behavior.<sup>[48]</sup> In order to create DNA-addressable printed structures, 1% (w/v) DNA-functionalized superlow melt agarose (HP45.1, Carl Roth, Germany) was additionally mixed into bioink with a doubled percentage in gelatin and alginate to reach the same polymer composition as in unmodified bioink. Functionalization of agarose with ssDNA strands was performed following the procedure described in ref. [33] prior to mixing of the polymers to the bioink (a detailed protocol for the bioink preparation is given in the Supporting Information).

**Sample Preparation:** DNA samples were prepared by mixing ssDNA ( $10 \times 10^{-6}$  M) in 1× TAE 1 M NaCl buffer with heated bioink (42 °C) to a final concentration of  $2.5 \times 10^{-6}$ – $5 \times 10^{-6}$  M (cf. Supporting Information).

**Sample Bioprinting:** Mixed bioink was degassed in a sonicator at 40 °C for 48 h prior to printing. Directly before printing, the bioink was placed into an oven or onto a thermoblock at 42 °C for 15 min and loaded in a glass syringe in the printhead preheated to the printing temperature. Extrusion on glass slides was performed with nozzles (Vieweg, Germany) of sizes from G22 (ID 410 μm) to G32 (ID 110 μm). After printing, the extruded structures were treated with 20 μL ddH<sub>2</sub>O to prevent drying, and swelling was allowed with 20 μL of 1× TAE + 1 M NaCl before DNA samples were added. Directly after the addition of DNA samples, the printed structure was sealed and imaging was started. For imaging, an epifluorescence microscope (Nikon Ti2-E) equipped with a 4× objective was employed. For larger structures (>2 mm), multipoint imaging and consecutive stitching with 50% overlap of single images were performed.

## Supporting Information

Supporting Information is available from the Wiley Online Library or from the author.

## Acknowledgements

The authors gratefully acknowledge support by the European Research Council (project AEDNA, grant no. 694410). The authors thank Elisabeth Falgenhauer for useful discussions and support during the construction of the 3D gel printer.

## Conflict of Interest

The authors declare no conflict of interest.

## Keywords

bioprinting, DNA nanotechnology, molecular programming

Received: March 19, 2020

Revised: May 18, 2020

Published online: June 29, 2020

- [1] M. R. Jones, N. C. Seeman, C. A. Mirkin, *Science* **2015**, 347, 1260901.
- [2] P. W. Rothmund, *Nature* **2006**, 440, 297.
- [3] S. M. Douglas, H. Dietz, T. Liedl, B. Hogberg, F. Graf, W. M. Shih, *Nature* **2009**, 459, 414.
- [4] F. C. Simmel, B. Yurke, H. R. Singh, *Chem. Rev.* **2019**, 119, 6326.
- [5] F. C. Simmel, R. Schulman, *MRS Bull.* **2017**, 42, 913.
- [6] J. Zheng, J. J. Birktoft, Y. Chen, T. Wang, R. Sha, P. E. Constantinou, S. L. Ginell, C. Mao, N. C. Seeman, *Nature* **2009**, 461, 74.
- [7] E. Stahl, F. Praetorius, C. C. de Oliveira Mann, K. P. Hopfner, H. Dietz, *ACS Nano* **2016**, 10, 9156.
- [8] H. Qi, M. Ghodousi, Y. Du, C. Grun, H. Bae, P. Yin, A. Khademhosseini, *Nat. Commun.* **2013**, 4, 2275.
- [9] K. F. Wagenbauer, C. Sigl, H. Dietz, *Nature* **2017**, 552, 78.
- [10] T. Zhang, C. Hartl, K. Frank, A. Heuer-Jungemann, S. Fischer, P. C. Nickels, B. Nickel, T. Liedl, *Adv. Mater.* **2018**, 30, 1800273.
- [11] A. J. Kim, P. L. Biancaniello, J. C. Crocker, *Langmuir* **2006**, 22, 1991.
- [12] D. Nykpanchuk, M. M. Maye, D. van der Lelie, O. Gang, *Nature* **2008**, 451, 549.
- [13] M. E. Leunissen, R. Dreyfus, F. C. Cheong, D. G. Grier, R. Sha, N. C. Seeman, P. M. Chaikin, *Nat. Mater.* **2009**, 8, 590.
- [14] M. R. Jones, R. J. Macfarlane, B. Lee, J. Zhang, K. L. Young, A. J. Senesi, C. A. Mirkin, *Nat. Mater.* **2010**, 9, 913.
- [15] Y. Wang, Y. Wang, X. Zheng, E. Ducrot, J. S. Yodh, M. Weck, D. J. Pine, *Nat. Commun.* **2015**, 6, 7253.
- [16] W. B. Rogers, V. N. Manoharan, *Science* **2015**, 347, 639.
- [17] Y. Zhang, A. McMullen, L. L. Pontani, X. He, R. Sha, N. C. Seeman, J. Brujic, P. M. Chaikin, *Nat. Commun.* **2017**, 8, 21.
- [18] J. S. Kahn, Y. Hu, I. Willner, *Acc. Chem. Res.* **2017**, 50, 680.
- [19] F. Li, J. Tang, J. Geng, D. Luo, D. Yang, *Prog. Polym. Sci.* **2019**, 98, 101163.
- [20] Y. Li, Y. D. Tseng, S. Y. Kwon, L. D'Espaux, J. S. Bunch, P. L. McEuen, D. Luo, *Nat. Mater.* **2004**, 3, 38.
- [21] S. H. Um, J. B. Lee, N. Park, S. Y. Kwon, C. C. Umbach, D. Luo, *Nat. Mater.* **2006**, 5, 797.
- [22] N. Park, S. H. Um, H. Funabashi, J. Xu, D. Luo, *Nat. Mater.* **2009**, 8, 432.
- [23] J. B. Lee, S. Peng, D. Yang, Y. H. Roh, H. Funabashi, N. Park, E. J. Rice, L. Chen, R. Long, M. Wu, D. Luo, *Nat. Nanotechnol.* **2012**, 7, 816.
- [24] Y. Xing, E. Cheng, Y. Yang, P. Chen, T. Zhang, Y. Sun, Z. Yang, D. Liu, *Adv. Mater.* **2011**, 23, 1117.
- [25] J. Jin, Y. Xing, Y. Xi, X. Liu, T. Zhou, X. Ma, Z. Yang, S. Wang, D. Liu, *Adv. Mater.* **2013**, 25, 4714.
- [26] Z. Xing, A. Caciagli, T. Cao, I. Stoev, M. Zupkauskas, T. O'Neill, T. Wenzel, R. Lamboll, D. Liu, E. Eiser, *Proc. Natl. Acad. Sci. USA* **2018**, 115, 8137.
- [27] C. Yao, H. Tang, W. Wu, J. Tang, W. Guo, D. Luo, D. Yang, *J. Am. Chem. Soc.* **2020**, 142, 3422.

- [28] J. Tang, C. Yao, Z. Gu, S. Jung, D. Luo, D. Yang, *Angew. Chem., Int. Ed.* **2020**, 59, 2490.
- [29] D. C. Lin, B. Yurke, N. A. Langrana, *J. Biomech. Eng.* **2004**, 126, 104.
- [30] T. Liedl, H. Dietz, B. Yurke, F. Simmel, *Small* **2007**, 3, 1688.
- [31] C. Li, A. Faulkner-Jones, A. R. Dun, J. Jin, P. Chen, Y. Xing, Z. Yang, Z. Li, W. Shu, D. Liu, R. R. Duncan, *Angew. Chem., Int. Ed.* **2015**, 54, 3957.
- [32] J. Thiele, Y. Ma, D. Föschepoth, M. M. Hansen, C. Steffen, H. A. Heus, W. T. Huck, *Lab Chip* **2014**, 14, 2651.
- [33] L. Aufinger, F. C. Simmel, *Angew. Chem., Int. Ed.* **2018**, 57, 17245.
- [34] Y. Hu, J. S. Kahn, W. Guo, F. Huang, M. Fadeev, D. Harries, I. Willner, *J. Am. Chem. Soc.* **2016**, 138, 16112.
- [35] A. Cangialosi, C. Yoon, J. Liu, Q. Huang, J. Guo, T. D. Nguyen, D. H. Gracias, R. Schulman, *Science* **2017**, 357, 1126.
- [36] P. B. Allen, Z. Khaing, C. E. Schmidt, A. D. Ellington, *ACS Biomater. Sci. Eng.* **2015**, 1, 19.
- [37] T. Hosoya, I. Kawamata, S.-I. M. Nomura, S. Murata, *New Gener. Comput.* **2019**, 37, 97.
- [38] M. Vaezi, H. Seitz, S. Yang, *Int. J. Adv. Manuf. Technol.* **2013**, 67, 1721.
- [39] R. L. Truby, J. A. Lewis, *Nature* **2016**, 540, 371.
- [40] S. V. Murphy, A. Atala, *Nat. Biotechnol.* **2014**, 32, 773.
- [41] A. B. Dababneh, I. T. Ozbolat, *J. Manuf. Sci. Eng.* **2014**, 136, 277.
- [42] K. Holzl, S. Lin, L. Tytgat, S. Van Vlierberghe, L. Gu, A. Ovsianikov, *Biofabrication* **2016**, 8, 032002.
- [43] J. Huang, S. Liu, C. Zhang, X. Wang, J. Pu, F. Ba, S. Xue, H. Ye, T. Zhao, K. Li, Y. Wang, J. Zhang, L. Wang, C. Fan, T. K. Lu, C. Zhong, *Nat. Chem. Biol.* **2019**, 15, 34.
- [44] L. M. Gonzalez, N. Mukhitov, C. A. Voigt, *Nat. Chem. Biol.* **2020**, 16, 126.
- [45] G. Villar, A. D. Graham, H. Bayley, *Science* **2013**, 340, 48.
- [46] M. Bayoumi, H. Bayley, G. Maglia, K. T. Sapra, *Sci. Rep.* **2017**, 7, 45167.
- [47] S. Doose, H. Barsch, M. Sauer, *Biophys. J.* **2007**, 93, 1224.
- [48] R. A. Rezende, P. J. Bártolo, A. Mendes, R. M. Filho, *J. Appl. Polym. Sci.* **2009**, 113, 3866.